JURNAL ILMIAH FLASH
Vol. 8 No. 2, Halaman: 81 - 88
Desember 2022

DESIGN OF HEAT EXCHANGER FOR THE PRODUCTION OF SYNTHESIS PBO PARTICLES

Tabita Dwi Vena[1], Asep Bayu Dani Nandiyanto[2]*, Risti Ragadhita[3], dan Teguh Kurniawan[4]
[1,2,3] Departemen Pendidikan Kimia, Universitas Pendidikan Indonesia
Jl. Dr. Setiabudi No.229 Kota Bandung, Jawa Barat 40154
[4] Teknik Kimia, Universitas Ageng Tirtayasa
Jl. Raya Palka No.Km 3, Kabupaten Serang, Banten 42124
* E-mail: nandiyanto@upi.edu

Abstract
This study aims to develop and analyze the design of heat exchangers (HE) in the synthesis of PbO particles using a single precursor method. This type of HE shell and tube one-pass is designed to be simple. The specifications of HE equipment are shell length 1.5200 m, shell diameter 0.1361 m, outer tube diameter 0.0334 m, and thickness 0.0243 m. Then the calculation is done manually using the Microsoft Excel application. The results showed that the HE shell and tube design with the one pass type has a laminar flow, with an effective value of 84.66%. Therefore, this heat exchanger with shell and tube one meets the requirements and standards based on effectiveness, but without considering the fouling factor. The results of this analysis can be used as a learning medium in the design process, analysis of heat exchanger performance, and operating mechanisms.

Kata kunci: Shell and tube, Heat exchanger, Effectiveness, PbO particle, Education.

INTRODUCTION

Heat exchanger is an apparatus for transferring heat between two or more fluids that are separated by an appropriate wall and have different temperatures [1]. Many different types of industries utilize heat exchangers to transfer heat between various fluids in order to recover waste heat and lower utility costs. The efficiency of heat exchangers is greatly influenced by the thermal and physical characteristics of the heat transfer fluids [2]. The industrial processing of PbO particles is one use for the heat exchanger.

Many uses for PbO particles, including for filler for silicon rubber [3], batteries [4], electrode [5], optoelectronic device [6], membrane [7], memristor [8], resin [9,10], pigment [11], catalyst [12].

Various approaches have been developed for the synthesis of PbO particles, including ball milling-annealing method [13], physical vapor deposition method [14], chemical bath deposition method [15], and single precursor method [16].

Several studies on the design of heat exchangers have been conducted [17-28]. In contrast to the studies mentioned, we analyze and evaluate the processes. Consequently, the purpose of this research is to design a heat exchanger to produce PbO particles. The designed heat exchanger is shell and tube type. This study is expected to be a useful reference in designing heat exchangers, as well as a learning and teaching method starting from the design process, working mechanisms, to performance.

METHODS

(1) Synthesis of PbO particles

The specific processing conditions and preparation procedures are shown in Figure 1. The procedure is adopted from the experiments of M. Nafees, et al [16]. To begin, $PbCl_2$ and $H_2C_2O_4$ are dissolved in distilled water under vigorous stirring at room temperature. Then, white precipitate of lead oxalate (PbC_2O_4) was formed which was collected and washed with absolute ethanol and distilled water several times to remove the traces of impurities. After that, PbC_2O_4 was dried by aging for 7 h at 60 °C. To make the oxide, dry PbC_2O_4 was heated for 3 h at 425 °C in a muffle furnace. After cooling naturally to room temperature, red-colored PbO was formed and collected for characterization. Chemical reactions involved in the synthesis are:

$$H_2C_2O_4 + PbCl_2 \rightarrow PbC_2O_4 + 2HCl$$
$$PbC_2O_4 \rightarrow PbO + CO_2 + CO$$

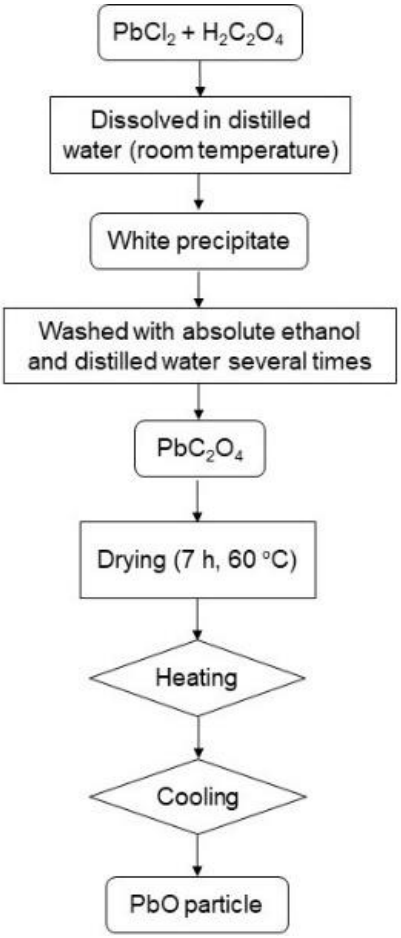

Fig. 1. Schematic diagram of the PbO particle preparation process using the co-precipitation method.

(2) Mathematical model for designed heat exchanger

The hot fluid used is oleic acid, while the cold fluid is water. The hot fluid enters at 450 °C and leaves at a temperature of 25 °C. The cold fluid enters at 20 °C and leaves at 90 °C. The assumptions used for the fluid characteristics operating in the heat exchanger is shown in Table 1. The incoming oleic acid flow rate is 3 (kg/s) while the incoming water flow rate is 2 (kg/s). In data collection, the Tubular Exchanger Manufacturers Association (TEMA) Standard was used as the reference regarding the specifications, while the thermal analysis is in the form of manual calculations using the basic Microsoft Excel application based on equations 1-27, follow what has been done by Nandiyanto, et al [29]. The heat exchange parameters that were calculated is shown in Table 2.

Table 1. Assumptions of fluid characteristics working on heat exchanger.

	Shell side	Tube side
	Hot fluid	Cold fluid
Inlet Temperature, T_{in} (K)	450	20
Outlet Temperature, T_{out} (K)	25	90
Fluid Flow Rate (kg/s)	3	2
Operating Pressure (atm)	1	1
Specific Heat (kJ/kg.K)	2,386	4,179
Density (kg/m^3)	895	1000

Table 2. Calculation of heat exchanger parameters.

Section	Parameters	Equation	Eq
Basic parameters	Energy transferred (Q)	$Q_{in} = Q_{out}$ $m_h \times C_{ph} \times \Delta T_h = m_c \times C_{pc} \times \Delta T_c$	(1)
	Logarithmic mean temperature differenced ($LMTD$)	$LMTD = \frac{(T_{hi}-T_{ci})-(T_{ho}-T_{co})}{In\frac{(T_{hi}-T_{ci})}{(T_{ho}-T_{co})}}$ where T_{hi}= inlet hot fluid temperature (°C) T_{ci}= inlet cold fluid temperature (°C) T_{ho}= outlet hot fluid temperature (°C) T_{co}= outlet cold fluid temperature (°C)	(2)
	Correction factor	$R = \frac{T_{hi}-T_{ho}}{T_{ci}-T_{co}}$	(3)
		$P = \frac{T_{hi}-T_{ho}}{T_{ci}-T_{co}}$	(4)
		$F = \frac{\sqrt{R^2+1}\,In\left[\frac{1-P}{1-PR}\right]}{(R-1)In\left(\frac{2-P(R+1-\sqrt{R^2+1})}{2-P(R+1+\sqrt{R^2+1})}\right)}$	(5)
	Heat Transfer Field Area (A)	$A = \frac{Q}{U \times LTMD}$ where Q = energy transfer (W) $LMTD$ = logarithmic mean temperature difference U = overall heat transfer coefficient	(6)
	Number of tubes (N)	$N = \frac{A}{\pi \times D_0 \times l}$ where N = number of tubes A = the area of the heat transfer area (m^2) π = 3,14 D_0 = tube diameter (m) l = tube length (m)	(7)
	Shell Diameter (D_s)	$D_s = 0{,}63\left(\frac{\sqrt{\frac{CL}{CTP}} \times (A \times PR^2 \times D_0)}{L}\right)^{1/2}$ where D_s = shell diameter (m) A = the area of the heat transfer area (m^2) P, R = correction factor D_0 = tube diameter (m) CTP = one tube (0,93); two tubes (0,90); three tubes (0,85) CL = 90° and 45° = 1,00; 30° and 60° = 0,87	(8)
Tube	Total Heat Transfer Surface Area in Tube (a_t)	$a_t = N_t \frac{a'_t}{n}$ where a_t = total heat transfer surface area in the tube (m^2) N_t = number of tubes a'_t = the flow area in the tube (m^2) n = number of passes	(9)
	Mass Flow Rate of Water in Tube (G_t)	$G_t = \frac{m_h}{a_t}$ where G_t = mass flow of water in the tube (kg/m^2s) m_h = mass flow rate of hot fluid (kg/s) a_t = total heat transfer surface area in the tube (m^2)	(10)

	Reynolds number (Re_t)	$Re_t = \frac{di_t \times G_t}{\mu}$ where Re_t = the Reynolds number in tube di_t =the inner tube diameter (m) G_t = the mass flow of water in the tube (m^2) μ = the dynamic viscosity (kg/ms)	(11)
	Prandtl Number (Pr_t)	$Pr_t = \left(\frac{C_p \times \mu}{K}\right)^{1/2}$ where Pr = Prandtl number C_p = the specific heat of the fluid in the tube μ = the dynamic viscosity of the fluid in the tube (kg/ms) K = the thermal conductivity of the tube material (W/m°C)	(12)
	Nusselt number (Nu_t)	$Nu_t = 0{,}023 \times {Re_t}^{0,6} \times Pr^{0,33}$	(13)
	Inside coefficient (hi)	$hi = \frac{Nu \times K}{d_{i,}t}$ where hi = the convection heat transfer coefficient in the tube (W/m^2°C) K = the thermal conductivity of the material (W/m°C) $d_{i,}t$ = the inner tube diameter (m)	(14)
Shell	Shell flow area (A_s)	$A_s = \frac{d_s \times C \times B}{P_t}$	(15)
		$D_b = d_0 \left(\frac{N_t}{k_1}\right)^{\frac{1}{n_1}}$ where d_s = shell diameter (m) C = clearance (P_t-d_0) B = a shell bundle P_t = tube pitch (1,25× d_0) (m)	(16)
	Mass Flow Rate of Water in Shell (Gs)	$Gs = \frac{m_c}{a_s}$ where m_c = the mass flow rate of the cold fluid (kg/s) a_s = the shell flow area (m^2)	(17)
	Equivalent diameter (d_e)	$d_e = \frac{4\left(\frac{Pt}{2} \times 0{,}87Pt - \frac{1}{2}\pi\frac{d_{o,t}}{4}\right)}{\frac{1}{2}\pi d_{o,t}}$ where Pt = tube pitch (1,25× d_0) (m) π = 3,14 $d_{o,t}$ = tube outside diameter (m)	(18)
	Reynold number (Re_s)	$Re_s = \frac{di_s \times Gs}{\mu}$ where Re_s = Reynold number di_s = inner tube diameter (m) Gs = the mass flow of water in the shell (kg/m^{2}s) μ = the dynamic viscosity (kg/ms)	(19)
	Prandtl Number (Pr_s)	$Pr_s = \left(\frac{C_p \times \mu}{K}\right)^{1/2}$	(20)

	Nusselt number (Nu_s)	$Nu_s = 0{,}023 \times {Re_s}^{0,6} \times Pr^{0,33}$ Where Re_s = Reynold number Pr = Prandtl number	(21)
	Convection Heat Transfer Coefficient (h_0)	$h_0 = \frac{Nu \times K}{d_e}$ where ho = convection heat transfer coefficient (W/m²°C) K = thermal conductivity (W/m°C) d_e = equivalent diameter (m)	(22)
Shell and Tube	Actual Overall Heat Transfer Coefficient (U_{act})	$U_{act} = \frac{1}{\frac{1}{h_i}+\frac{\Delta r}{k}+\frac{1}{h_o}}$ where h_i = inside heat transfer coefficient (W/m²°C) h_o = outside heat transfer coefficient (W/m²°C), Δr = wall thickness (m) k = thermal conductivity(W/m°C)	(23)
Heat rate	Hot Fluid Rate (C_h)	$C_h = m_h \times Cp_h$ where C_h = hot fluid rate (W/°C) Cp_h = specific heat capacity (J/kg°C) m_h = mass flow rate of hot fluid (kg/s)	(24)
	Cold Fluid Rate (C_c)	$C_c = m_c \times Cp_c$ where C_c = cold fluid rate (W/°C) Cp_c = specific heat capacity (J/kg°C) m_c = mass flow rate of cold fluid (kg/s) $Q_{max} = C_{min}(T_{h,i} - T_{c,i})$ where Q_{max} = maximum heat transfer (W) C_{min} = minimum heat capacity rate (W/°C) $T_{h,i}$ = temperature of the hot fluid inlet (°C) $T_{c,i}$ = temperature of the cold fluid inlet (°C)	(25)
Effectiveness	Heat Exchanger Effectiveness (ε)	$\varepsilon = \frac{Q_{act}}{Q_{max}} \times 100\%$ where Q_{act} = actual energy transferred (W) Q_{max} = maximum heat transfer (W)	(26)
	Number of Transfer Unit (NTU)	$NTU = \frac{U \times A}{C_{min}}$ where U = overall heat transfer coefficient (W/m²°C A = heat transfer area (m2) C_{min} = minimum heat capacity rate (W/°C)	(27)

RESULTS AND DISCUSSION

RESULT

The complete calculation results are shown in Table 3.

Table 3. Heat Exchanger performance parameters designed based on calculations.

No.	Parameter	Results
1	Initial Heat Transfer Rate (Q)	3042762 W
2	Logarithmic Mean Temperature Difference ($LMTD$)	196.8292 °C
3	Assumed Overall Fluid Heat Coefficient of Water (U_a)	700 W/m^2.K
4	Area of Heat Transfer (A)	39.2601 m^2
5	Number of Tube (Nt)	88
6	Total Heat Transfer Surface Area in Tube (a_t)	0.4475 m^2
7	Mass Flow Rate of Water Fluid in Tube (Gt)	340.3423 kg/ m^2.s
8	Reynold Number in Tube (Re,t)	212.71
9	Prandtl Number in Tube (Pr,t)	359.38
10	Nusselt Number in Tube (Nu,t)	20.69
11	Convection Heat Transfer Coefficient in the Tube (h_i)	27028 W/m^2.K
12	Bundle Shell (Db)	0.3651 m
13	Total Heat Transfer Surface Area in Shell (a_s)	0.4475 m^2
14	Mass Flow Rate of Water Fluid in Shell (Gs)	216.4127 kg/ m^{2}s
15	Equivalent Diameter (De)	44674.7899 m
16	Reynold Number in Shell (Re,s)	10803658.29
17	Prandtl Number in Shell (Pr,s)	6.25
18	Nusselt Number in Shell (Nu,s)	23805.58
19	Convection Heat Transfer Coefficient in Shell (h_o)	6255936 W/m^2.K
20	Overall Heat Transfer Coefficient Actual (U_{act})	10.0731 W/m^2.K
21	HE Effectiveness (ε)	84.66%
22	Number of Transfer Unit (NTU)	3.3814

DISCUSSION

The calculation shows that the transferred energy value (Q) is 3042762 W with a shell length of 1.5200 m, a shell diameter of 0.1361 m, an inner diameter of 0.0160 m, and an outer diameter of 0.0334 m. The wall thickness, tube length and tube pitch were 0.0243 m, 4.2672 m, 0.0277 m; respectively. The effectiveness of heat exchanger was found to be 84.66% which indicates the actual heat transfer rate that was divided by the maximum heat transfer rate. The total heat exchanger performance is also determined by the specific heat of the fluid, density viscosity, and thermal conductivity.

The designed heat exchanger design model is shown in Fig. 2. PbO synthesis requires a heating temperature of 450 °C and then cooled at room temperature in the range of 20-25 °C. Therefore, the hot fluid used is oleic acid and the cold fluid is water. The hot fluid enters at a temperature of 450 °C and leaves at a temperature of 25 °C. The cold fluid enters at 20 °C and leaves at 90 °C. After a red particle formed, the process to production the PbO particle has finished.

Therefore, this heat exchanger with shell and tube one meets the requirements and standards based on effectiveness, but without the calculation of the fouling factor.

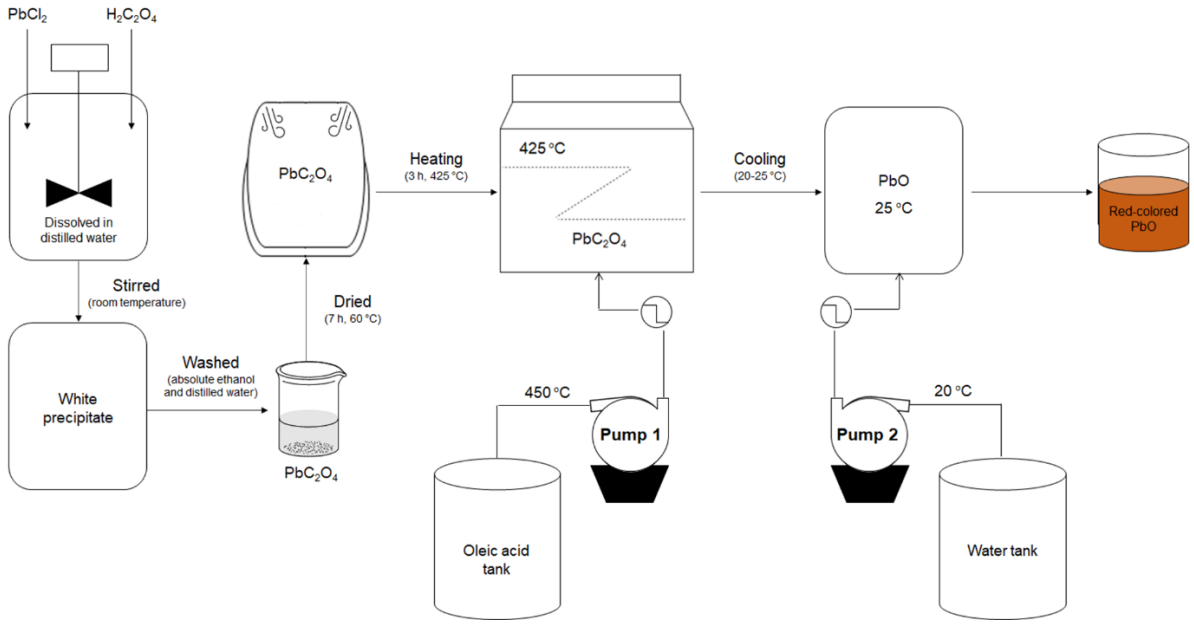

Figure 2. PFD on the synthesis of PbO particles.

CONCLUSION

Calculation of the heat exchanger specifications obtained shell length of 1.5200 m, shell diameter of 0.1361 m, inner diameter of 0.0160 m, outer tube diameter of 0.0334 m, wall thickness of 0.0243 m, tube length 4.2672 m, and tube pitch 0.0277 m. Based on the calculations performed through Microsoft Excel, the results show that the heat exchanger design on the shell and tube that fits is a laminar flow type, with an effectiveness of 84.66%. Therefore, this heat exchanger with shell and tube one meets the requirements and standards based on effectiveness, but without the calculation of the fouling factor.

ACKNOWLEDGMENTS

This study was supported by Dr. Eng. Asep Bayu Dani Nandiyanto, ST., M. Eng and Dr. Teguh Kurniawan, ST., MT. The author grateful for the advice and knowledge provided during the writing of this article.

REFERENCES

[1]. Zohuri, B. (2017). Heat exchanger types and classifications. In Compact Heat Exchangers (pp. 19-56). Springer, Cham.
[2]. Fares, M., Mohammad, A. M., & Mohammed, A. S. (2020). Heat transfer analysis of a shell and tube heat exchanger operated with graphene nanofluids. Case Studies in Thermal Engineering, 18, 100584.
[3]. El-Khatib, A. M., Abbas, M. I., Hammoury, S. I., Gouda, M. M., Zard, K., & Elsafi, M. (2022). Effect of PbO-nanoparticles on dimethyl polysiloxane for use in radiation shielding applications. Scientific Reports, 12(1), 1-13.
[4]. Das, H. J., Shah, A., Singh, L. R., & Mahato, M. (2021). Waste derived low cost PbO-Carbon nanocomposite and its energy storage application. Materials Today: Proceedings, 47, 1072-1077.
[5]. Zhou, Q., Zhou, X., Zheng, R., Liu, Z., & Wang, J. (2021). Application of Lead Oxide Electrodes in Wastewater Treatment: A Review. Science of The Total Environment, 150088.
[6]. Gunasekaran, M., & Seenuvasakumaran, P. (2021). Lead oxide and vanadium doped lead oxide thin films for optoelectronic device applications. *Materials Today: Proceedings*, *47*, 1114-1118.
[7]. Hamid, A., Khan, M., Hayat, A., Raza, J., Zada, A., Ullah, A., ... & Hussain, F. (2020). Probing the physio-chemical appraisal of green synthesized PbO nanoparticles in PbO-PVC nanocomposite polymer membranes. *Spectrochimica Acta Part A: Molecular and Biomolecular Spectroscopy*, *235*, 118303.
[8]. Perla, V. K., Ghosh, S. K., & Mallick, K. (2020). Carbon nitride supported lead oxide nanoparticles for memristor application: Charge-transport mechanism for resistive switching. *The Journal of Physical Chemistry C*, *125*(1), 1054-1059.
[9]. Ghaseminejad, M., Gholamzadeh, L., & Ostovari, F. (2021). Investigation of x-ray attenuation property of modification PbO with graphene in epoxy polymer. *Materials Research Express*, *8*(3), 035008.
[10]. Sabri, J. H., & Mahdi, K. H. (2019). A

Comparative Study for Micro and Nano shield of (PbO) composite for gamma Radiation. *Energy Procedia*, *157*, 802-814.

[11]. Araújo, V. D. D., Andreeta, M. R. B., Maia, L. J. Q., Nascimento, R. M. D., Motta, F. V. D., Bomio, M. R. D., ... & Bernardi, M. I. B. (2015). Microstructural, structural and optical properties of nanoparticles of PbO-CrO 3 pigment synthesized by a soft route. *Cerâmica*, *61*, 118-125.

[12]. Hashemi, L., Morsali, A., Yilmaz, V. T., Büyükgüngor, O., Khavasi, H. R., Ashouri, F., & Bagherzadeh, M. (2014). Sonochemical syntheses of two nano-sized lead (II) metal–organic frameworks; application for catalysis and preparation of lead (II) oxide nanoparticles. *Journal of Molecular Structure*, *1072*, 260-266.

[13]. Yazdan, A., Hu, B., Nan, C. W., & Li, L. (2021). Synthesis of polycrystalline boron nitride nanotubes with Lead (II) oxide and Iron (III) nitrate nonahydrate as promoters. *Physica E: Low-dimensional Systems and Nanostructures*, *133*, 114788.

[14]. Abdulrahman, A. F., Mohammed, R. Y., Ahmed, S. M., & Hamad, S. M. (2021). Synthesis of lead oxide thin films by using physical vapor deposition technique. *Materials Today: Proceedings*, *42*, 2752-2755.

[15]. Ahmed, S. M., Mohammed, R. Y., Abdulrahman, A. F., Ahmed, F. K., & Hamad, S. M. (2021). Synthesis and characterization of lead oxide nanostructures for radiation attenuation application. *Materials Science in Semiconductor Processing*, *130*, 105830.

[16]. Nafees, M., Ikram, M., & Ali, S. (2017). Thermal stability of lead sulfide and lead oxide nano-crystalline materials. *Applied Nanoscience*, *7*(7), 399-406.

[17]. Cuce, E., Guclu, T., & Cuce, P. M. (2020). Improving thermal performance of thermoelectric coolers (TECs) through a nanofluid driven water to air heat exchanger design: An experimental research. *Energy Conversion*

[18]. Nguyen, T. K., Sheikholeslami, M., Jafaryar, M., Shafee, A., Li, Z., Chandra Mouli, K. V., & Tlili, I. (2020). Design of heat exchanger with combined turbulator. *Journal of Thermal Analysis and Calorimetry*, *139*(1), 649-659.

[19]. Wang, W., Li, Y., Zhang, Y., Li, B., & Sundén, B. (2020). Analysis of laminar flow and heat transfer in an interrupted microchannel heat sink with different shaped ribs. *Journal of Thermal Analysis and Calorimetry*, *140*(3), 1259-1266.

[20]. Kwon, B., Liebenberg, L., Jacobi, A. M., & King, W. P. (2019). Heat transfer enhancement of internal laminar flows using additively manufactured static mixers. *International Journal of Heat and Mass Transfer*, *137*, 292-300.

[21]. Mortean, M. V. V., & Mantelli, M. B. H. (2019). Nusselt number correlation for compact heat exchangers in transition regimes. *Applied Thermal Engineering*, *151*, 514-522.

[22]. Shi, H., Raimondi, N. D. M., Fletcher, D. F., Cabassud, M., & Gourdon, C. (2019). Numerical study of heat transfer in square millimetric zigzag channels in the laminar flow regime. *Chemical Engineering and Processing-Process Intensification*, *144*, 107624.

[23]. Song, K., Tagawa, T., Chen, Z., & Zhang, Q. (2019). Heat transfer characteristics of concave and convex curved vortex generators in the channel of plate heat exchanger under laminar flow. *International Journal of Thermal Sciences*, *137*, 215-228.

[24]. Saydam, V., Parsazadeh, M., Radeef, M., & Duan, X. (2019). Design and experimental analysis of a helical coil phase change heat exchanger for thermal energy storage. *Journal of Energy Storage*, *21*, 9-17.

[25]. Zhang, P., Rong, X., Yang, X., & Zhang, D. (2019). Design and performance simulation of a novel hybrid PV/T-air dual source heat pump system based on a three-fluid heat exchanger. *Solar energy*, *191*, 505-517.

[26]. Saltzman, D., Bichnevicius, M., Lynch, S., Simpson, T. W., Reutzel, E. W., Dickman, C., & Martukanitz, R. (2018). Design and evaluation of an additively manufactured aircraft heat exchanger. *Applied Thermal Engineering*, *138*, 254-263.

[27]. Yang, H., Wen, J., Wang, S., & Li, Y. (2018). Effect of fin types and Prandtl number on performance of plate-fin heat exchanger: Experimental and numerical assessment. *Applied Thermal Engineering*, *144*, 726-735.

[28]. Zhang, P., Ma, T., Li, W. D., Ma, G. Y., & Wang, Q. W. (2018). Design and optimization of a novel high temperature heat exchanger for waste heat cascade recovery from exhaust flue gases. *Energy*, *160*, 3-18.

[29]. Nandiyanto, A. B. D., Putri, S. R., Ragadhita, R., & Kurniawan, T. (2022). Design of Heat Exchanger for The Production of Carbon Particles. Journal of Engineering Science and Technology, 17(4), 2788-2798.